COMBINED EFFECTS OF GRAVITY, BENDING MOMENT, BEARING CLEARANCE, AND INPUT TORQUE ON WIND TURBINE PLANETARY GEAR LOAD SHARING

Researchers from the National Renewable Energy Laboratory share a paper they presented at the American Gear Manufacturers Association Fall Technical Meeting in October 2012.

By: Yi Guo, Jonathan Keller, and William LaCava

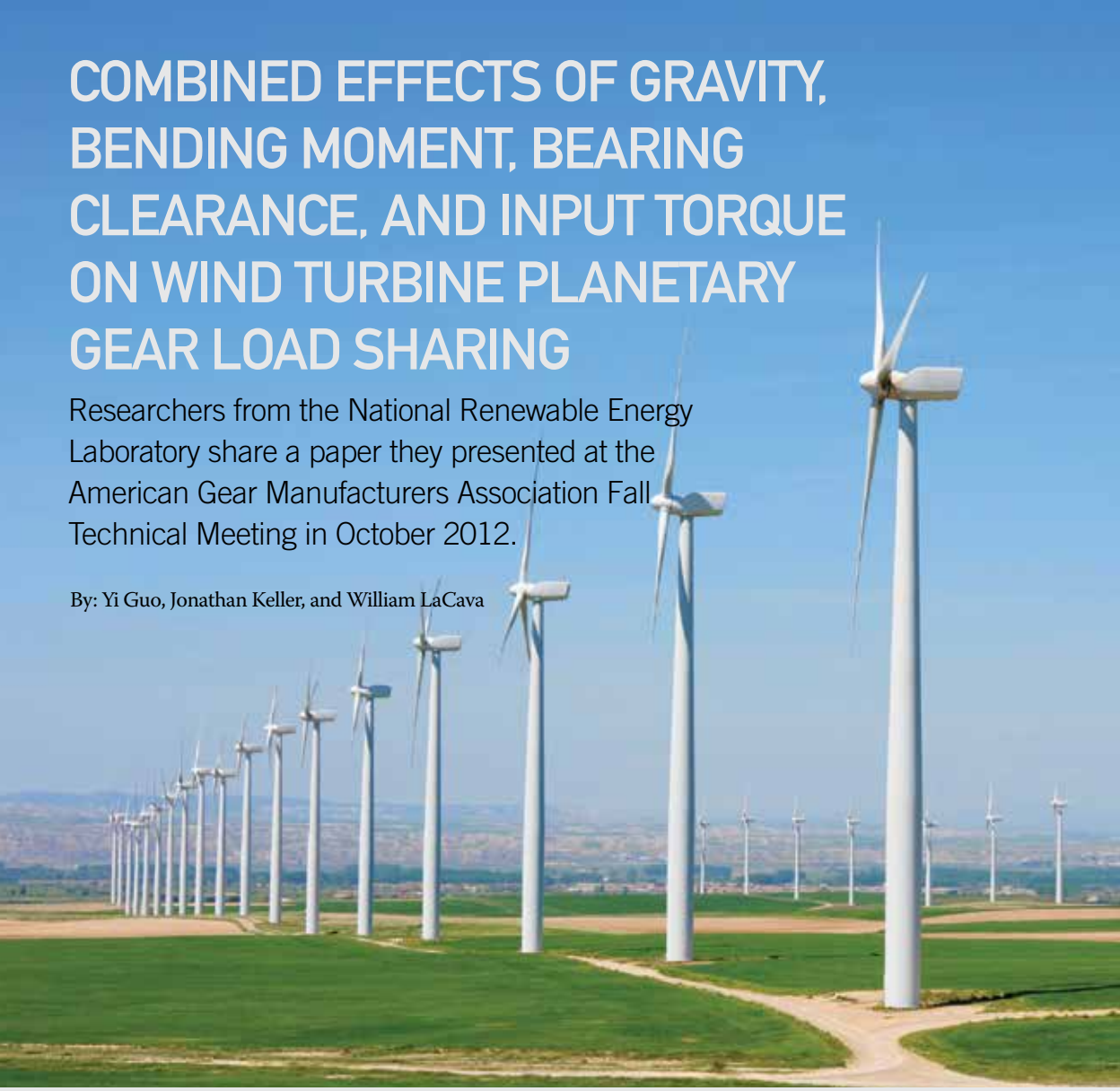

Jonathan Keller is a senior engineer and Yi Guo is a postdoctoral researcher with the National Wind Technology Center, a research facility of the National Renewable Energy Laboratory. William LaCava is a Ph.D. student at the UMass Amherst. For more information, visit www.nrel.gov/nwtc.

ABSTRACT

This computational work investigates planetary gear load sharing of three-mount suspension wind turbine gearboxes. A three-dimensional multibody dynamic model is established, addressing gravity, bending moments, fluctuating mesh stiffness, nonlinear tooth contact, and bearing clearance. A flexible main shaft, planetary carrier, housing, and gear shafts are modeled using reduced degrees-of-freedom through modal condensation. This drivetrain model is validated against the experimental data of the Gearbox Reliability Collaborative for gearbox internal loads.

Planet load sharing is a combined effect of gravity, bending moment, bearing clearance, and input torque. Influences of each of these parameters and their combined effects on the resulting planet load sharing are investigated. Bending moments and gravity induce fundamental excitations in the rotating carrier frame, which can increase gearbox internal loads and disturb load sharing. Clearance in carrier bearings reduces the bearing stiffness, and thus the bending moment from the rotor can be transmitted into gear meshes. With bearing clearance, the bending moment can cause tooth micropitting and can induce planet bearing fatigue,

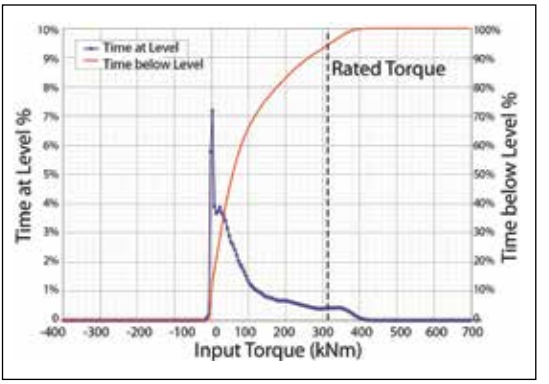

Figure 1: Torque distribution throughout measurement campaign on NEG Micon NM48/750 turbine [2,18].

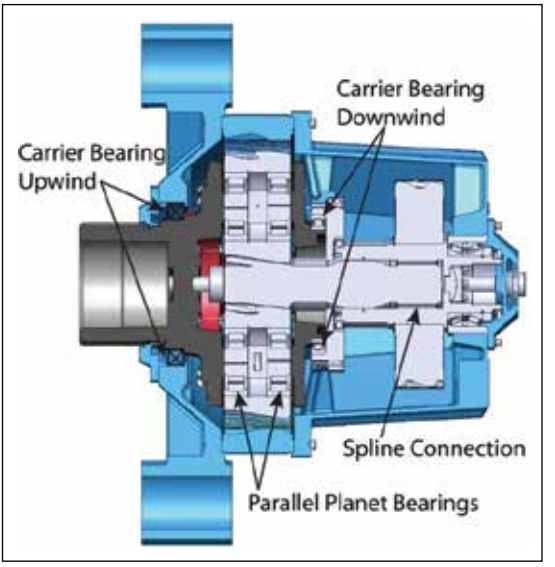

Figure 2: Cut-view of the GRC gearbox configuration.

leading to reduced gearbox life. At low input torque, planet bearings are susceptible to skidding. At rated torque and beyond, planet bearings are at risk of fatigue.

INTRODUCTION

Wind turbines have traditionally experienced premature gearbox failures [1]. The cost of gearbox rebuilds, as well as the down time associated with these failures, has elevated the cost of wind energy. The National Renewable Energy Laboratory Gearbox Reliability Collaborative (GRC) was established by the U.S. Department of Energy in 2006; its key goal is to understand the root causes of premature gearbox failures and improve their reliability using a combined approach of dynamometer testing, field testing, and modeling [2]. A major modeling activity of the GRC is to evaluate assumptions and uncertainties in current design practices that could affect gearbox reliability. As a part of the GRC program, this paper investigates planetary gear load-sharing in three-mount suspension wind turbine drivetrains that affects the load path and gearbox component life.

Compared to parallel axis gears, planetary gear systems provide high power density by splitting the input torque into multiple, parallel sun-planet and ring-planet load paths. Planetary gear systems are commonly used in wind turbine drivetrains and they use nearly or exactly equally-spaced planet gears, theoretically leading to equally shared

Figure 3: 750 kW wind turbine drivetrain of NREL GRC.

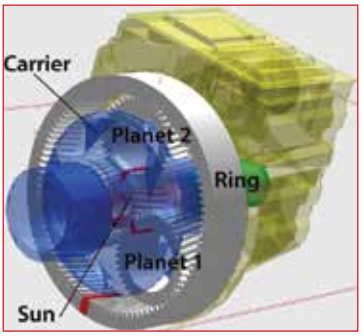

Figure 4: (a) Side view and (b) axial view of the multi-body model of the examined gearbox with flexible carrier and housing.

loads at each planet. However, in reality planet gear loads are not always equally shared among planets [3,4,5,6,7,8,9,10,11]. With unequally shared loads, planet bearing forces increase, leading to reduced bearing life and potential premature failure. Planetary gear load sharing is an important design parameter for drivetrain reliability. The degree of unequal load sharing has implications for tolerance schemes and gearbox loads.

Early studies by Hidaka and Terauchi [3] investigated disturbed load sharing by manufacturing and assembly errors on a Stoekicht planetary gear. This unequal load sharing was not significant when the mesh frequency was lower than 1000 Hz. Hayashi et al. [5] developed a method to measure the planet gear shearing stress and studied the influences of gear tooth profile error and eccentricity on load sharing. Ligata el al. [6] investigated the effect of pin position error on planet load sharing and a method for computing the planet load sharing from root strain-time histories was proposed. Singh [12] found that the tangential pin position error has a greater effect on the load sharing compared to the radial error. It was also shown that the sensitivity to pin position error increases as the number of pinions in the planetary gear set increases [6,12]. Singh [13,14] developed a formulation to estimate load sharing considering the unequal planet spacing for three to seven planetary gears. The analytically predicted load sharing factor was compared against a finite element analysis using the program developed by Vijayakar [15].

Various techniques have been investigated to improve load sharing. Studies show using a flexible ring gear improved load sharing when a number of manufacturing and assembly errors were present [4,16]. Kahraman et al. investigated the effects of ring gear flexibility on planetary gear loads using a finite element model and experiments and found contradictory results [10,17]. They found that adding flexibility to the ring gear was not as effective as a floating sun in improving load sharing. Kahraman [9] developed a two-dimensional lumped-parameter model to calculate tooth and bearing loads of planetary gears. The study also investigated the effect of a floating sun on load sharing and found it did not improve disturbed load sharing due to pin position errors. Similar results were shown in the study by Singh [12].

This aforementioned research on load sharing is limited to unequally spaced planets due to manufacturing errors and eccentricity. Input torque is considered as the only applied load to these planetary gears in prior studies. Nearly all horizontal-axis wind turbine gearboxes carry various combinations of input torque and non-torque loads. The non-torque loads include bending moments caused by the rotor weight and tower shadow, wind induced moments, moments caused by the controller, thrust, etc. Three-mount suspension drivetrains studied by NREL GRC show significant bending moment on the main shaft, which is mainly caused by the rotor weight and aerodynamic forces [2]. This bending moment has the same order of magnitude as input torque [2,18]. Other wind turbine designs adopt a two main bearing configuration to reduce the transmission of these non-torque loads into gearboxes. These turbines still have a small amount of bending moment present on the main shaft.

The measured load spectrum of the GRC turbine considering various wind and weather conditions is shown in Figure 1. Over 90% of the time, the GRC wind turbine operates below rated torque. Within the entire load spectrum, the turbine operates below 10% of rated torque over 50% of testing period. Gearbox reliability at low input torque has received little attention in the past because prior research has mainly focused on the low bearing and tooth loads with low input torque. Influences of bending moment are not considered for the low load conditions.

With the increasing size of wind turbines, gravity induced excitation in the rotating carrier frame becomes an important vibration source. Gravity led to tooth wedging, a potential source for premature planet bearing failure, in a wind turbine planetary gear investigated by Guo and Parker [19]. Clearance is introduced in rolling element bearings to account for thermal expansion, interference fit, and surface roughness during operation. Clearances in wind

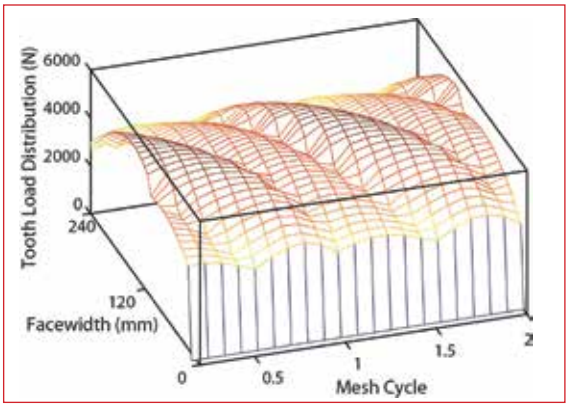

Figure 5: Tooth load distribution with profile and lead modification at .the sun-planet 1 mesh.

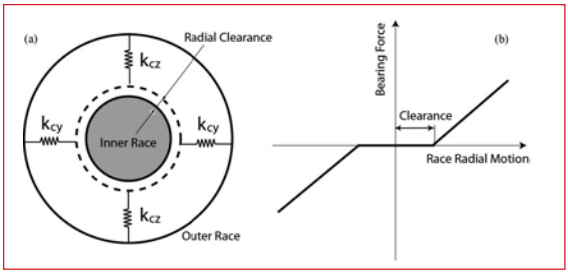

Figure 6: Nonlinear bearing model.

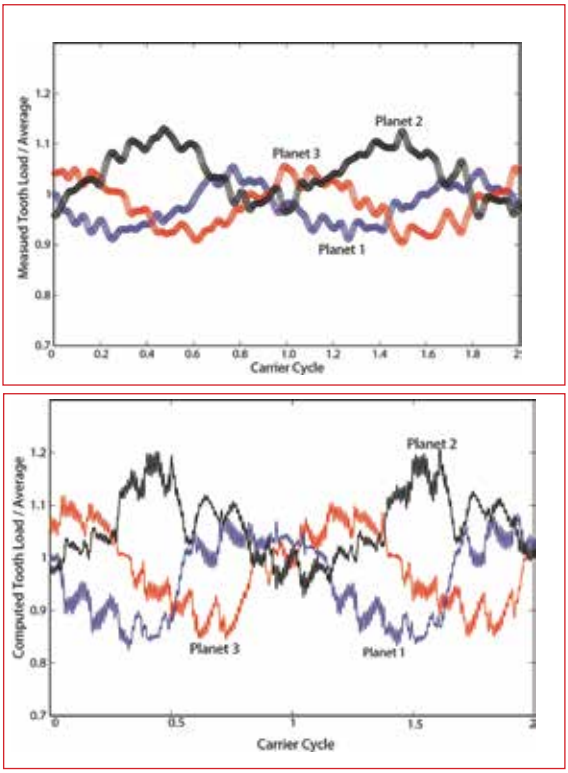

Figure 7: (a, top) Measured during the dynamometer testing; (b, bottom) calculated planetary load sharing at rated torque.

turbine bearings are large and can cause gear tooth misalignment, leading to uneven tooth and bearing load distribution and increased bearing vibration [19, 20, 21].

This study investigates the combined effects of gravity, bending moment, bearing clearance, and input torque on planetary load sharing of three-mount suspension wind turbine gearboxes. Gearbox internal loads at low input torque--a wind turbine operating condition that is rarely considered--are also studied under effects of bending moment.

GRC WIND TURBINE DRIVETRAIN DESCRIPTION

This study investigates the 750 kW turbine drivetrain used by the NREL GRC. This drivetrain has a spherical roller main bearing that supports the main shaft and rotor weight, and two trunnion mounts that support the gearbox. The gearbox includes a helical planetary stage with three equally-spaced planets and two parallel stages, with stage ratios of 5.71, 3.57, and 4.00, respectively. The rated input speed is 22.2 rpm. A cut-away view of the gearbox is shown in Figure 2. There are two parallel carrier bearings supporting the carrier. Each planet gear is supported by two identical cylindrical bearings. The sun shaft is connected to the intermediate shaft through a spline connection with 300 μm backlash to partially float the sun. The ring is bolted to the gearbox housing. This drivetrain configuration represents the majority of the existing three-mount suspension wind turbine drivetrains. Key parameters of the planetary section are listed in Table 1 and Table 2 (Appendix). Additional details of this gearbox are described in the literature [22].

EXPERIMENTAL SETUP AND INSTRUMENTATION

The GRC project instrumented two identical 750 kW wind turbine gearboxes for dynamometer (Figure 3) and field testing. Internal measurements include gear tooth loads, main shaft torque and bending, internal component deflections and misalignments, and planet bearing loads. The full description of instrumentation is detailed in [2].

Main shaft torque and bending were measured using three sets of strain gauges in full bridge arrangements. These measurements are taken near the center of the main shaft between the main bearing and gearbox [2]. The shaft torque and bending measurement serves as a reference for the input load being applied to the gearbox from the rotor side, and can also be used as the time series input for dynamic simulations. The bending moments caused by the blades and hub weight and aerodynamic forces were measured in the field tests, and are 29.2% to 64.6% of rated input torque [2].

For each planet bearing, three axial slots were machined into the inner diameter of the inner ring

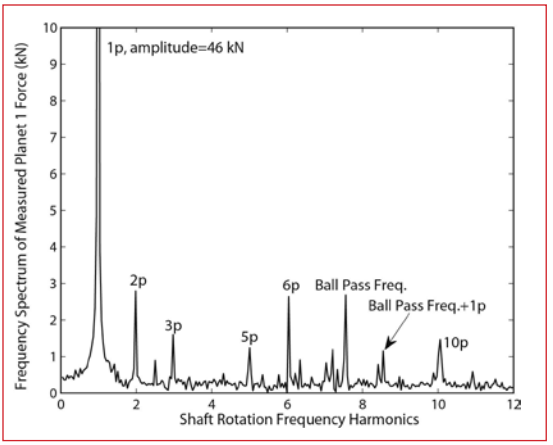

Figure 8: FFT spectrum of the measured planet 1 bearing force in the tangential direction.

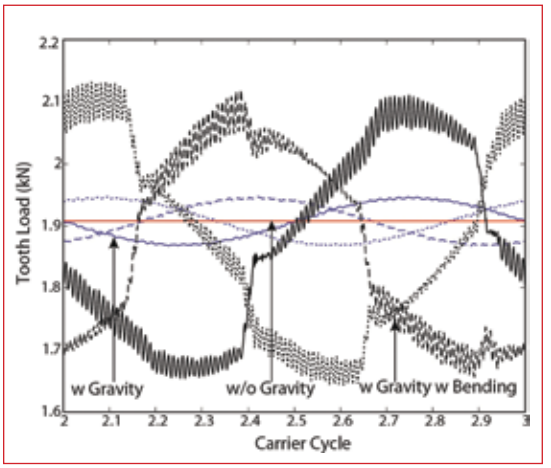

Figure 9: Dynamic tooth loads at the 1st sun-planet (–), 2nd sun-planet (––), and 3rd sun-planet (···) meshes without gravity and bending moment (red), with gravity (blue), and with gravity and bending moment (black). Carrier bearing clearance is 275 μm. Planet bearing clearance is 0.

and instrumented with strain and temperature gauges [2]. Two of the slots were located at different locations in the bearing load zone for each planet, and the third slot for every bearing was oriented 90° from the sun-planet axis, referred to here as top dead center (TDC). Two gauge sets in each TDC slot and two bearings on each planet provided an axial distribution of four radial loads along each planet pin. These gauges were calibrated to loads applied to the fully assembled planet pins and bearing pairs in a bench top test setup [23].

DYNAMIC DRIVETRAIN MODELING

The three-dimensional dynamic model of the wind turbine drivetrain is established in SIMPACK [24]. This model includes the main shaft, low speed planetary gear, planetary carrier, and housing as shown in Figure 4(a) and Figure 4(b). The parallel stages are not included in this study.

Gears are modeled as rigid bodies with six degrees-of-freedom x, y, z, θ_x, θ_y *and* θ_z. The gear contact analysis considers the time varying tooth meshing when the gears rotate by modeling the fluctuating mesh stiffness according to the AGMA 6006 standard [25]. The gears are modeled using a slicing approach to determine the load distribution across the gear tooth facewidth, which accounts for tooth profile and lead modification, tooth contact loss, and fluctuating mesh stiffness. The tooth load distribution of the sun gear teeth with tooth modifications is shown in Figure 5. This model also considers shuttling contact and sliding friction forces [26].

Bearings are modeled using diagonal stiffness matrices. Radial bearing clearance is included in the model as shown in Figure 6. Radial forces develop only when the relative displacement between the connected bodies exceeds a specified clearance. For instance, the radial forces of the carrier bearings are

$$(1)\ f_c^j = \mu_{cj} k_{cj} (\| j_c - j_h \| - \Delta_c), j = y, z$$

where $k_{cj}, j = y, z$ are the bearing stiffnesses. j_c, j_h are the displacements of the carrier and housing. The variable $\mu_{cj}, j = y, z$ tracks if the bearings are in contact according to

$$(2)\ \mu_{cj} = \begin{cases} 1 & \text{if} \quad (j_c - j_h) > \Delta_c \\ -1 & \text{if} \quad (j_c - j_h) < -\Delta_c \\ 0 & \text{if} \quad \| j_c - j_h \| < \Delta_c \end{cases}$$

The model includes the flexibilities of the main shaft, planet carrier, shafts, and gearbox housing, which are important structural components in the drivetrain that could affect gear dynamics. The gearbox front and rear housings and planet carrier are included as reduced finite element flexible bodies. Finite element models are created in Abaqus and reduced using the Craig-Bampton method [27]. Master degrees-of-freedom, referred to here as "nodes", are selected at each interface point. For the planet carrier, nodes at the main shaft connection, upwind and downwind carrier bearing connections, the planet-pin upwind and downwind bores, and planet pins are retained for the drivetrain model. Housing nodes were retained at each bearing location, the ring gear interface center, and the yoke mount centers. All the eigenfrequencies below 1,000 Hz of the housing and carrier are included for the super element creation in Abaqus. This cut-off frequency (1,000 Hz) is selected to include higher than 25th harmonic of the planetary stage mesh frequency at rated speed. After creating the super elements and performing modal analyses on the reduced matrices, the flexible bodies are imported into the multibody drivetrain model. The ring is modeled as a rigid body due to software limitations. Shafts are modeled using beam elements.

The sun spline connection is modeled using its diagonal stiffness matrix obtained through a finite element analysis

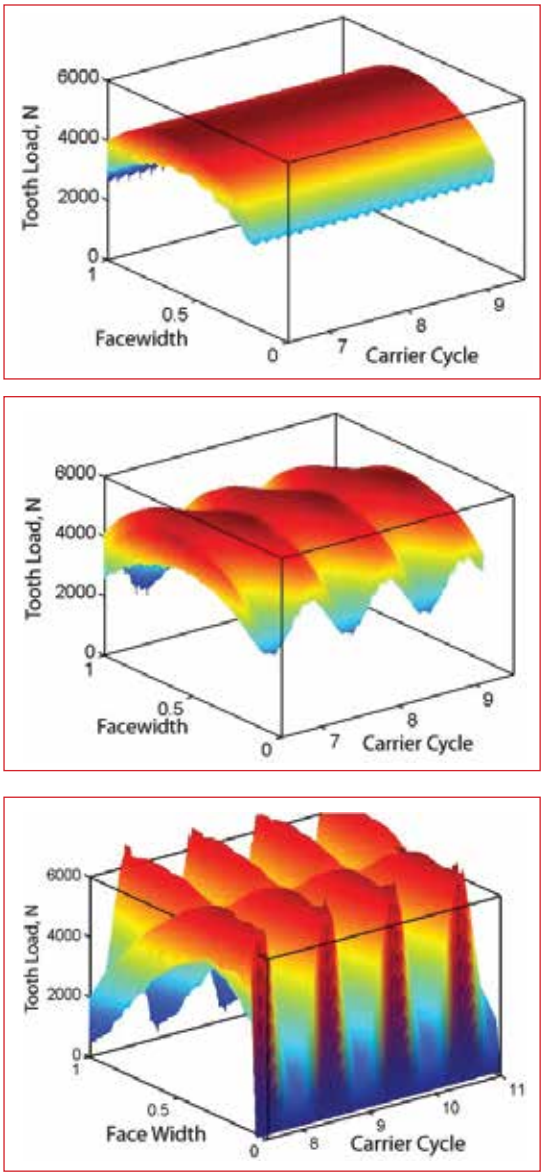

Figure 10: Tooth load distribution on the sun-planet mesh (a) without gravity and bending moment; (b) with carrier bearing clearance with gravity; (c) with clearance, gravity, and bending moment (10% of measured moment) at rated torque. Carrier bearing clearance is 275 μm. Planet bearing clearance is 0.

in RomaxWIND [28] (Table 4 in the Appendix). Spline facewidth, crowning, applied load, and surface lubrication affect these stiffnesses. Trunnion mounts are modeled using diagonal stiffness matrices extracted from the measured load-displacement curve [2].

MODEL VALIDATION BY EXPERIMENTS

A steady state dynamic analysis is carried out on the established model using the Newmark method at the rated speed. A step size of 1 ms is selected to include the first 10 harmonics of planetary gear mesh frequency. All components are allowed to vibrate. An average of 5%

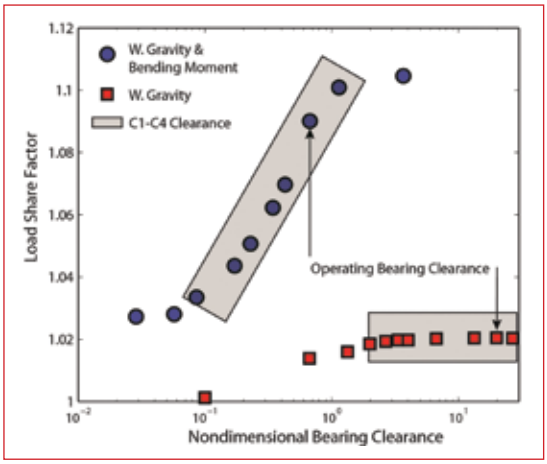

Figure 11: Load sharing factor sensitivity to carrier bearing clearance computed using the established model with gravity effect only (■) and with gravity and bending moment (●). Carrier bearing clearance is 275 μm. Planet bearing clearance is 0.

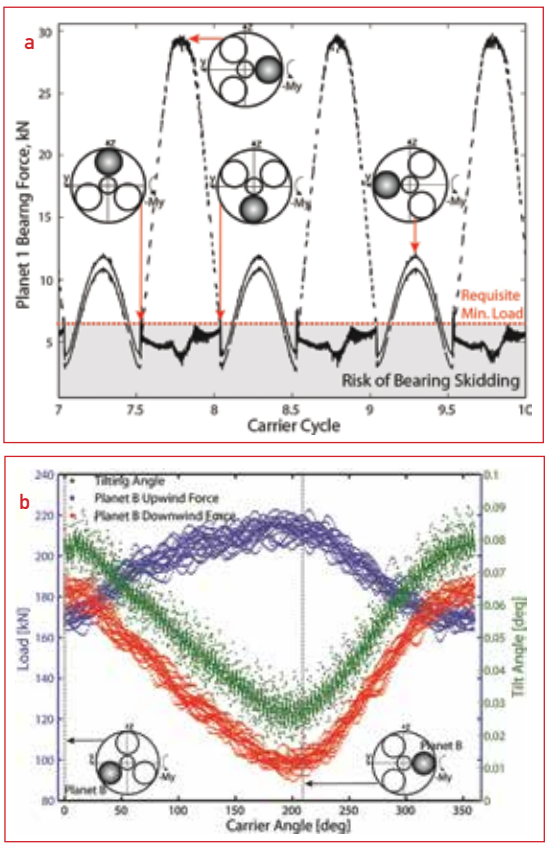

Figure 12: (a) Calculated upwind (––) and downwind (–) planet bearing loads at 5% of rated torque; (b) measured planet tilting angle and bearing loads at rated torque. Carrier bearing clearance is 275 μm. Planet bearing clearance is 0.

modal damping is used. Applied torque to the main shaft ranges from 35 *kNm* to 350 *kNm*. The measured bending moment is applied to the carrier.

The load sharing factor often refers to the ratio between the maximum and the average bearing force among planets [29] .

$$(3)\quad k_\gamma(t) = \max\left\{f_p^i(t)\right\}_i \Big/ mean\left\{mean\left[f_p^i(t)\right]_i\right\}_t, i = 1,\ldots,N$$

where $f_p^i(t)$ is the planet i bearing force that includes the upwind and downwind rows and N is the number of planets.

This load sharing factor defined in Eq. (3) is a function of time. This study uses the maximum value of $k_\gamma(t)$ over time, defined as

$$(4)\quad k_\gamma^* = \max\left[k_\gamma(t)\right]_t$$

The computational results are compared to the measured planetary load sharing in Figure 7(a) and Figure 7 (b). Results show the load sharing factor exceeds 1.1 with disrupted load sharing. The calculated load sharing among planets agrees with the measured data in general. The fluctuating amplitude of load sharing factor is slightly different between the computed results and measurements. The measured shaft moment is applied to the carrier in the drivetrain model. Due to the main shaft weight, the shaft moment measured at the carrier during the experiment is about 15% lower than that at the measurement location. Different excitation sources during the measurement and simulation also contribute to this difference. Figure 8 shows the frequency spectrum of the measured planet bearing force. Measurement data is filtered with low sampling frequency that did not capture mesh frequency 36.7 Hz and its higher harmonics. The drivetrain model does not include the bearing excitation due to its stiffness variation with roller kinematic rotation that was observed during the experiments as shown in Figure 8.

The maximum load of planet 2 over a carrier revolution is higher than the other planets due to the asymmetry of planet spacing during operation, which is seen in both measured and calculated results (Figure 7). This planet asymmetry is caused by planet bearing clearance and tangential pin position error.

Tooth loads at the sun-planet and ring-planet meshes create significant tangential bearing forces under operating torques, which have the same order of magnitude as tooth loads. Planet bearings are in contact when gears are loaded under most operating conditions except at vibration resonances with tooth contact loss [21]. Planet bearing clearance, however, disturbs the planet symmetry by introducing tangential position error, leading to asymmetric shared loads among planets over time as shown in Figure 7 (a) and Figure 7 (b). With identical planet bearing clearance,

Figure 13: A cylindrical planet bearing with sliding marks in the circumferential direction [32].

planet bearing forces have identical shapes with only phase differences. The measurements in Figure 7 (a) are achieved by introducing planet bearing clearances in the drivetrain model (Figure 4). Bearing clearances in planets 1, 2, and 3 are 179 μm; 80 μm; and 179 μm, respectively that are chosen based on the measured clearances by the GRC project [30]. Figure 7 (b) can be regenerated by disturbing the mounting angles of planets by $\alpha_i = \delta_p^i / d_c$, where d_c is the center distance and δ_p^i is planet bearing clearance. Having a planet bearing clearance different from other planet bearings has the same effects on load sharing as tangential pin position error.

RESULTS AND DISCUSSION

Excitations Caused by Gravity and Bending Moment

With a rotating planetary carrier, the gravity force on a planetary gear is periodic in the rotating carrier frame. The gravity force vector is

$$(5)\quad \mathbf{f}_g(t) = \left[G_n \sin(\gamma), -G_n \sin(\Omega_c t)\cos(\gamma), -G_n \cos(\Omega_c t)\cos(\gamma)\right]$$

where $G_n, n = c, r, s, p$ denote the gravity forces of the carrier, ring, sun, and planet, respectively. Ω_c is the carrier rotation frequency and γ is the bedplate tilt angle.

The bending moment vector in the rotating carrier frame is

$$(6)\quad \mathbf{M}(t) = \left[0, -M_y \sin(\Omega_c t), -M_y \cos(\Omega_c t)\right]$$

The effects of gravity and bending moment on tooth loads are shown in Figure 9. Without considering gravity, tooth loads at different sun-planet meshes are nearly identical and time-invariant. Gravity causes the fluctuation of tooth loads by disturbing the system symmetry. The tooth load at the $l^{th}, l = 2, \ldots N$ sun-planet mesh has a phase difference of $2\pi(l-1)/N$ compared to that at the first sun-planet mesh. When the bending moment is considered, the tooth load fluctuation becomes significant and the maximum tooth load increases 11% compared to its nominal value. The high frequency content ($99\times\Omega_c$ and $198\times\Omega_c$) of the tooth load with bending moment in Figure 9 is caused by fluctuating mesh stiffness that is the dominant internal excitation.

Figure 10 shows the effects of gravity and bending moment on tooth load distribution. Without gravity and bending moment, tooth contact has a time-invariant, parabolic shape as shown in Figure 10(a). When gravity is included, the gear teeth carry the carrier weight, leading to a disturbed tooth load distribution. This tooth contact pattern changes periodically about carrier frequency. With bending moment, the load distribution is poor and the gear teeth have edge loading by carrying the bending moment and carrier weight. Excitations caused by gravity and bending moment in the rotating carrier frame are unavoidable for wind turbine gearboxes mounted in the horizontal axis. Bending moment plays an essential role in gearbox internal loads compared to gravity and the excitation from gear meshing.

Effect of Carrier Bearing Clearance on Load Transfer Path

In three-mount suspension drivetrains, carrier bearings are designed with a high load capacity to reduce the gearbox load sensitivity to non-torque loads such that gears only carry torque loads. Carrier bearing forces are one order of magnitude smaller than planet bearing forces because they are nearly balanced by almost self-equilibrating tooth loads at the sun-planet and ring-planet meshes. When the bearing clearance is larger than the carrier motion, the carrier bearings are not in contact during operation. Consequently, the gear teeth carry the non-torque loads and the carrier weight instead of the carrier bearings, resulting in cyclic tooth loads similar to Figure 9, Figure 10(b), and Figure 10(c). Clearance in carrier bearings plays an important role in this load path.

The variation of the load sharing factor (defined in Eq. (3)) with carrier bearing clearance is shown in Figure 11. The bearing clearance is nondimensionalized by dividing the motion amplitude of the carrier with infinite bearing clearance. When the bearing clearance is larger than the carrier motion, the load sharing factor converges to a constant, which indicates a limiting system with infinite bearing clearance. The load sharing factor increases 2% when carrier bearing clearance increases from 0 to 1 with gravity. With bending moment and gravity, the load sharing factor increases from 1.02 to 1.13 when bearing clearance increases. Without bearing clearance, the load sharing is nearly ideal. Reducing or eliminating this bearing clearance reduces

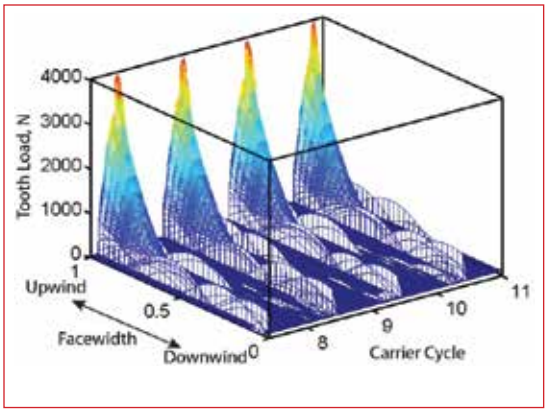

Figure 14: Tooth load distribution at the ring-planet 1 mesh when input torque is 5% of the rated. Carrier bearing clearance is 275 μm. Planet bearing clearance is 0.

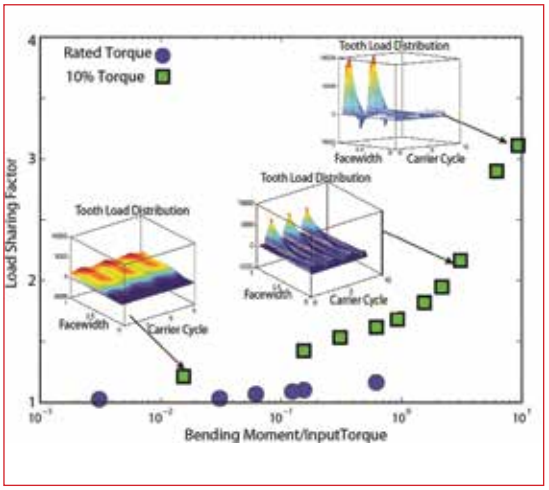

Figure 15: Load sharing factor sensitivity considering input torque, bending moment, gravity, and bearing clearance. Carrier bearing clearance is 275 μm. Planet bearing clearance is 0.

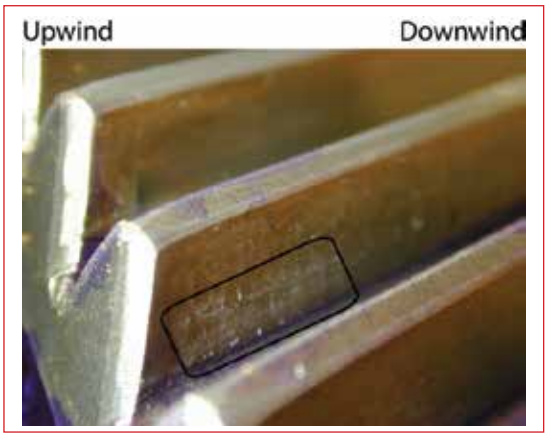

Figure 16: Ring gear teeth with edge loading.

gearbox load sensitivity to non-torque loads and improves load sharing.

The recommended bearing clearance within C1-C4 range according to AGMA 6006 standard [31] is larger than the carrier motion for the pure torque case. With the recommended bearing clearance, carrier bearings are lightly loaded or can be entirely out of contact during operation, leading to a reduced load carrying capacity. Calculating the nondimensional bearing clearance helps design the appropriate radial clearance for increasing the load capacity during operation.

Effects of Input Torque on Gearbox Internal Loading

The highest torque measured during a braking event in the field testing of the GRC gearbox is 189% of input torque [18]. Considering bending moment, results suggest that planet bearing loads at high input torque exceed the fatigue limit, which could lead to premature bearing failure.

When input torque is low, bending moment plays a dominant role in gearbox internal loads. Planet bearing loads of upwind and downwind rows at 5% torque are shown in Figure 12. The upwind planet bearing is heavily loaded compared to the downwind bearing over 50% time within a carrier cycle. The upwind bearing load reaches a maximum of 9.7 times the average load of the downwind planet bearing when the planet gear aligns with $-y$ direction (Figure 12 (a)). At this instant, the upwind planet bearing carries the majority of the bending moments while the downwind planet bearing carries much less. When this planet is moving away from the $-y$ axis and the next adjacent planet is moving towards $-y$, the load sharing of the prior planet at the upwind and downwind rows is nearly equal. This unequal load sharing between upwind and downwind rows of planet bearings was observed during the testing. Figure 12(b) shows the measured planet bearing loads and tilting angle (initially located at 210 degree counter-clockwise from $-y$) at rated torque. The upwind bearing load reaches the maximum when this planet aligns with $-y$, which agrees with the model prediction on the locations with highest upwind bearing loads as shown in Figure 12(a). This agreement qualitatively validates the model for capturing the load sharing between the upwind and downwind row bearings.

As shown in Figure 12(a), planet bearing loads are lower than the required minimum load for preventing rolling element sliding. Planet bearings are susceptible to skidding that

compromises the rolling integrity of the bearing, leading to a reduced bearing life. Typical planet bearing damage caused by skidding motion is shown in Figure 13. There is no skidding damage observed in the GRC gearbox because the gearbox was removed from service (due to other failure modes) long before skidding damage could develop.

Under the same loading condition of Figure 12(a), the tooth load distribution of the first ring-planet mesh is shown in Figure 14 When the upwind planet bearing carries majority of bending moments (carrier cycle from 7.5 to 8 in Figure 12 (a)), the gear tooth has edge contact towards upwind side and partial contact loss towards downwind side as shown in Figure 14. Unequal planet loads between upwind and downwind rows cause tooth edge loading.

Combined Effects on Load Sharing

Planetary gear load sharing relies on gravity, bending moment, bearing clearance, and input torque. Among them, bending moment and input torque are decisive parameters. A nondimensional quantity $M=M_y/T_{in}$ introduced here to consider the combined loading condition, where M_y is bending moment and T_{in} is input torque. Figure 15 shows the planetary gear load sharing with various values of M. Gravity and bearing clearances are included in the results. Load sharing is computed at 10% and rated torques. The load sharing-bending curve at 10% torque is higher than that with rated torque because the influence of gravity on load sharing factor is relatively higher at low input torque. Bending moment increases load sharing factor nearly linearly. A large bending moment induces nonlinear tooth contact, particularly at low input torque. At 10% torque, gear tooth load contact changes from slightly disturbed load distribution when the nondimensional bending moment is less than 0.02, to edge loading when it is larger than 0.02 and less than 2, and eventually reversing contact when it is larger than 2. With edge loading and reversing contact, gear teeth lose contact and reengage repeatedly over time. The time-varying tooth contact causes dynamic forces on planet bearings that could result in acceleration and deceleration of roller elements in entering and leaving the contact zone, thereby reducing bearing life.

Gear tooth edge loading has been observed during the GRC experiments as shown in Figure 16. Micropitting induced by the edge contact was evident at the upwind side of on the ring gear teeth, which agrees with the model predictions in Figure 14 and Figure 15. As found in both simulation and experiment, it is clear that the shaft bending moment has been transmitted from the rotor to the gears, which suggests the design assumption that non-torque loads are uncoupled from gearboxes is not valid.

CONCLUSIONS

A multibody dynamic drivetrain model was established to investigate planetary gear loads in wind turbine drivetrains. This model includes gravity, bending moments, tooth modification, fluctuating mesh stiffness, tooth contact loss, and bearing clearance. Unequal load sharing among planets and between upwind and downwind rows of each pair of planet bearings predicted by the established model agrees with the GRC dynamometer measurements. Planetary gear load sharing in three-mount suspension drivetrains depends on gravity, bending moment, bearing clearance, and input torque:

- Bending moments and gravity are fundamental external excitations for wind turbine planetary gears mounted in the horizontal-axis, leading to cyclical loading on gear teeth and planet bearings. They have stronger influences on planetary gear loads than fluctuating mesh stiffness. Bending moments cause unequal load sharing between upwind and downwind planet bearings, which can cause abnormal tooth contact consisting of tooth edge loading, partial contact loss, and reversing contact, resulting in tooth micropitting.
- Clearance in carrier bearings affects the gearbox load sensitivity to non-torque loads. With carrier bearing clearance, bending moment can transmit into gear meshes and planet bearings, leading to a reduced gearbox life. Planet bearing clearance has a similar effect on load sharing as tangential pin position error. It disturbs the symmetry of planets, leading to asymmetric bearing loads.
- At low input torque, the effects of bending moment on gearbox internal loads are dominant. Upwind planet bearing loads can be an order of magnitude higher than the downwind bearing loads. Planet bearings, in particular the downwind row, are at risk for skidding.

ACKNOWLEDGEMENTS

The authors thank Mark McDade, Brian McNiff, and Jeroen Van Dam for providing the pictures; the GRC team for valuable discussions throughout this study; Robert Solomon from SIMPACK, Inc. and Dr. Ashley Crowther from RomaxWIND Inc. for providing the software. The Gearbox Reliability Collaborative (GRC) project at the National Renewable Energy Laboratory is funded by the Wind and Water Power Program of the United States Department of Energy.

APPENDIX

	Sun	Planet	Ring
Number of Teeth	21	39	99
Pitch Diameter (*mm*)	215.6	400.4	1016.4
Root Diameter (*mm*)	186.0	372.9	-
Base Diameter (*mm*)	198.8	369.3	937.4
Whole Depth Constant	2.4	2.4	2.4
Tooth Thickness (*mm*)	16.84	18.80	8.55
Module (*mm*)	10.0	10.0	10.0
Helix Angle (^{0})	7.4947 (right)	7.4947 (left)	7.4947 (left)
Backlash (*mm*)	0.25/0.29	0.25/0.29	0.30/0.36
Pressure Angle	20.0^0		
Center Distance (*mm*)	308.0		

Table 1: Geometric Parameters of the Planetary Gear.

	Sun	Carrier	Planet	Ring	Housing
Mass (kg)	181.6	756.9	104.0	480.0	1213.0
$I_{xx}\ (kg \cdot m^2)$	1.26	59.1	3.20	144.2	340.0
$I_{yy}\ (kg \cdot m^2)$	24.0	60.3	2.04	75.4	554.4
$I_{zz}\ (kg \cdot m^2)$	24.0	60.3	2.04	74.4	424.8

Table 2: System Parameters of the Planetary Gear.

	Carrier (Up)	Carrier (Down)	Planet	Trunnion
$k_x\ (N/m)$	10^{12}	10^{12}	10^{12}	
$k_y\ (N/m)$	1.8×10^9	1.4×10^9	3.4×10^9	0.1×10^9
$k_z\ (N/m)$	1.8×10^9	1.4×10^9	3.4×10^9	0.1×10^9
$k^{\theta}_{q_x}\ (Nm/rad)$	0	0	0	0
$k^{\theta}_{q_y}\ (Nm/rad)$	55×10^3	27×10^3	0.53×10^6	0.54×10^6
$k^{\theta}_{q_z}\ (Nm/rad)$	55×10^3	27×10^3	0.53×10^6	0.54×10^6

Table 3: Bearing Information.

Radial, *N/m*	Axial, *N/m*	Tilting, *Nm/rad*	Rotational, *Nm/rad*
20×10^9	0	3.5×10^6	10×10^9

Table 4: Sun Spline Stiffness.

REFERENCES

[1] W. Musial, S. Butterfield and B. McNiff, "Improving wind turbine gearbox reliability," Milan, Italy, 2007.

[2] H. Link, W. LaCava, J. V. Dam, B. McNiff, S. Sheng, R. Wallen, M. McDade, S. Lambert, S. Butterfield and F. Oyague, "Gearbox reliability collaborative project report: findings from phase 1 and phase 2 testing," NREL technical report: NREL/TP-5000-51885, 2011.

[3] T. Hidaka, Y. Terauchi and K. Nagamura, "Dynamic behavior of planetary gear (1st report, load distribution in planetary gear)," in *Bulletin of JSME*, 1976.

[4] A. Kahraman and G. W. Blankenship, "Gear dynamics experiments, part ii: effect of involute contact ratio.," in *ASME Power Transmission and Gearing Conference*, San Diego, 1996.

[5] T. Hayashi, Y. X. Li, I. Hayashi, K. Endou and W. Watanabe, "Measurement and some discussions on dynamic load sharing in planetary gears.," in *Bulletin of JSME*, 1986.

[6] H. Ligata, A. Kahraman and A. Singh, "An experimental study of the influence of manufacturing errors on the planetary gear stresses and planet load sharing," *Journal of Mechanical Design*, vol. 130, pp. 041701-1, 2008.

[7] H. W. Muller, W. G. Mannhardt and J. H. Glover, Epicyclic Drive Trains: Analysis, Systhesis, Synthesis, and Applications, Detroit: Wayne State University Press, 1982.

[8] D. L. Seager, "Load sharing among planet gears," in *SAE Technical Paper*, 1970.

[9] A. Kahraman, "Load sharing characteristics of planetary transmissions," *Mechanism and Machine Theory*, vol. 29, no. 8, pp. 1151-1165, 1994.

[10] A. Kahraman and S. M. Vijayakar, "Effect of internal gear flexibility on the quasi-static behavior of a planetary gear set," *Journal of Mechanical Design*, vol. 123, no. 3, pp. 408-415, 2001.

[11] A. Bodas and A. Kahraman, "Influence of carrier and gear manufacturing errors on the static load sharing behavior of planetary gear sets," *JSME International Journal. Series C. Mechanical Systems, Machine Elements and Manufacturing*, vol. 47(3), pp. 908-915, 2004.

[12] A. Singh, "Application of a system level model to study the planetary load sharing behavior," *Journal of Mechanical Design*, vol. 127, pp. 469-476, 2005.

[13] A. Singh, "Load sharing behavior in epicyclic gears: Physical explanation and generalized formulation," *Mechanism and Machine Theory*, vol. 45, pp. 511-530, 2010.

[14] A. Singh, "Epicyclic load sharing map — development and validation," *Mechanism and Machine Theory*, pp. 632-646, 2011.

[15] S. M. Vijayakar, "A combined surface integral and finite-element solution for a 3-dimensional contact problem," *International Journal for Numerical Methods in Engineering*, vol. 31, no. 3, pp. 525-545, 1991.

[16] F. Cunliffe, J. D. Smith and D. B. Welbourn, "Dynamic tooth loads in epicyclic gears," *ASME Journal of Engineering for Industry*, vol. 5, no. 95, pp. 578-584, 1974.

[17] A. Kahraman, H. Ligata and A. Singh, "Influence of ring gear rim thickness on planetary gear set behavior," *Journal of Mechanical Design*, vol. 132, p. 021002, 2010.

[18] J. V. Dam, R. T. and E. Overly, "Torque measurements on GRC test turbine 1," NREL, 2007.

[19] Y. Guo and R. G. Parker, "Dynamic modeling and analysis of a spur planetary gear involving tooth wedging and bearing clearance nonlinearity," *European Journal of Mechanics A/Solids*, vol. 29, pp. 1022-1033, 2010.

[20] A. Crowther, A. Ramakrishnan, N. A. Zaidi and C. Halse, "Sources of time-varying contact stress and misalignments in wind turbine planetary sets," *Wind Energy*, vol. 14, no. 5, pp. 637-651, 2011.

[21] Y. Guo and R. G. Parker, "Dynamics of planetary gears with bearing clearance," *ASME Jounal of Computational Nonlinear Dynamics*, vol. 7, no. 3, p. 031008, 2012.

[22] F. Oyague, "NREL Gearbox Reliability Collaborative Analysis Round Robin," NREL/CP-500-45325, 2009.

[23] J. V. Dam, "Gearbox reliability collaborative bearing calibration," NREL/TP-5000-47852, 2011.

[24] SIMPACK. [Online]. Available: http://www.simpack.com/.

[25] AGMA 6006-A03: Design and specification of gearboxes for wind turbines, July 2009, AGMA, 2009.

[26] L. Mauer, "Force element 225 gear wheel," *Intec GmbH internal report*, 2005.

[27] R. R. Craig, "A review of time-domain and frequency-domain component mode synthesis method," *Journal of Modal Analysis*, vol. 2(2), pp. 59-72, 1985.

[28] "Romax Wind Software Suite," [Online]. Available: http://www.romaxtech.com.

[29] A. 6123-B06, Design manual for enclosed epicyclic gear drives, American Gear Manufacturers Association, 2006.

[30] W. LaCava and M. McDade, "Gearbox 1 Measurements Report," NREL, Preprint, 2011.

[31] AGMA, "AGMA 6006: Calculation of load capacity of spur and helical gears," 2006.

[32] T. E. Tallian, "Failure atlas for rolling bearings in wind turbines," 2011.